nature cell biology

AMPH-1/Amphiphysin/Bin1 functions with RME-1/Ehd1 in endocytic recycling

Saumya Pant[1], Mahak Sharma[3], Kruti Patel[1], Steve Caplan[3], Chavela M. Carr[2] and Barth D. Grant[1,4]

RME-1/EHD1 (receptor mediated endocytosis/Eps15 homology-domain containing 1) family proteins are key residents of the recycling endosome, which are required for endosome-to-plasma membrane transport in *Caenorhabditis elegans* and mammals. Recent studies suggest similarities between the RME-1/EHD proteins and the Dynamin GTPase superfamily of mechanochemical pinchases, which promote membrane fission. Here we show that endogenous *C. elegans* AMPH-1, the only *C. elegans* member of the Amphiphysin/BIN1 family of BAR (Bin1-Amphiphysin-Rvs161p/167p)-domain-containing proteins, colocalizes with RME-1 on recycling endosomes *in vivo*, that *amph-1*-deletion mutants are defective in recycling endosome morphology and function, and that binding of AMPH-1 Asn-Pro-Phe(Asp/Glu) sequences to the RME-1 EH-domain promotes the recycling of transmembrane cargo. We also show a requirement for human BIN1 (also known as Amphiphysin 2) in EHD1-regulated endocytic recycling. *In vitro*, we find that purified recombinant AMPH-1–RME-1 complexes produce short, coated membrane tubules that are qualitatively distinct from those produced by either protein alone. Our results indicate that AMPH-1 and RME-1 cooperatively regulate endocytic recycling, probably through functions required for the production of cargo carriers that exit the recycling endosome for the cell surface.

Previous work has shown that RME-1 and mammalian mRme-1/EHD1 are ATPases that require ATP binding for homo-oligomerization and function *in vivo*[1–4]. Like RME-1 and mRme-1/EHD1, the vertebrate-specific paralogues EHD2, EHD3 and EHD4 also function in endocytic transport, but at different steps[5–8]. Although not apparent from the primary sequence, recent structural analysis of EHD2 has revealed that its central ATP-binding 'G-domain' resembles the GTP-binding domain of the large GTPase Dynamin[9], a protein that mediates membrane fission through its ability to constrict vesicle necks[10,11]. Additional similarities between EHD2 and Dynamin have also been found, including the ability of EHD2 to assemble into spiral rings around acidic liposomes when bound to a non-hydrolysable ATP analogue[9]. It has been further shown that EHD2 ATPase activity is stimulated upon lipid binding and oligomerization, reminiscent of the assembly-stimulated GAP activity characteristic of Dynamin[9].

However, other than the G-domain, RME-1/EHD family proteins are distinct from established Dynamin superfamily members. RME-1/EHD family proteins lack pleckstrin homology (PH) domains. Rather, the primary lipid-binding region of EHD2 is helical, forming a unique scissor-like interface in the EHD2 dimer[9]. RME-1/EHD family proteins also lack proline-rich domains. Instead, RME-1/EHD family proteins contain a carboxy-terminal Eps15-homology (EH) domain, which is a different type of peptide-binding interface, known to target Asn-Pro-Phe-containing partner proteins[12,13]. Given the high degree of overall similarity among RME-1/EHD family members (about 65% sequence identity) and their recently identified similarity to Dynamin, it has been suggested that all RME-1/EHD family proteins could have Dynamin-like properties in promoting membrane fission[4,9]. In particular, because recycling receptors accumulate in endosomes in the absence of RME-1 or EHD1 (refs 1–3), RME-1/EHD1 could function as the fission machinery for tubules emanating from endosomes, promoting the release of transport carriers during receptor recycling events.

RESULTS

Identification of RME-1-interacting proteins

To gain greater insight into the role of RME-1 at the recycling endosome, we sought functional interactors that might aid RME-1 in the recycling process. Sequence alignment of several known binding partners of the mammalian EHD proteins has suggested that RME-1/EHD family EH-domains prefer Asn-Pro-Phe target sequences found in multiples and/or followed by acidic residues (reviewed in ref. 13). The acidic residues following an Asn-Pro-Phe sequence could potentially neutralize the unique positive surface charge near the Asn-Pro-Phe binding pocket of RME-1/EHD family EH-domains[13,14].

Using bioinformatic searches of the predicted *C. elegans* proteome, we identified 839 predicted worm proteins containing at least one Asn-Pro-Phe

[1]Department of Molecular Biology and Biochemistry, Rutgers University, Piscataway, NJ 08854, USA. [2]Department of Pathology and Laboratory Medicine, UMDNJ, Piscataway, NJ 08854, USA. [3]Department of Biochemistry and Molecular Biology, University of Nebraska Medical Center, Omaha NE 68198, USA. [4]Correspondence should be addressed to B.D.G. (e-mail: grant@biology.rutgers.edu).

Received 3 August 2009; accepted 6 October 2009; published online 15 November 2009; DOI: 10.1038/ncb1986

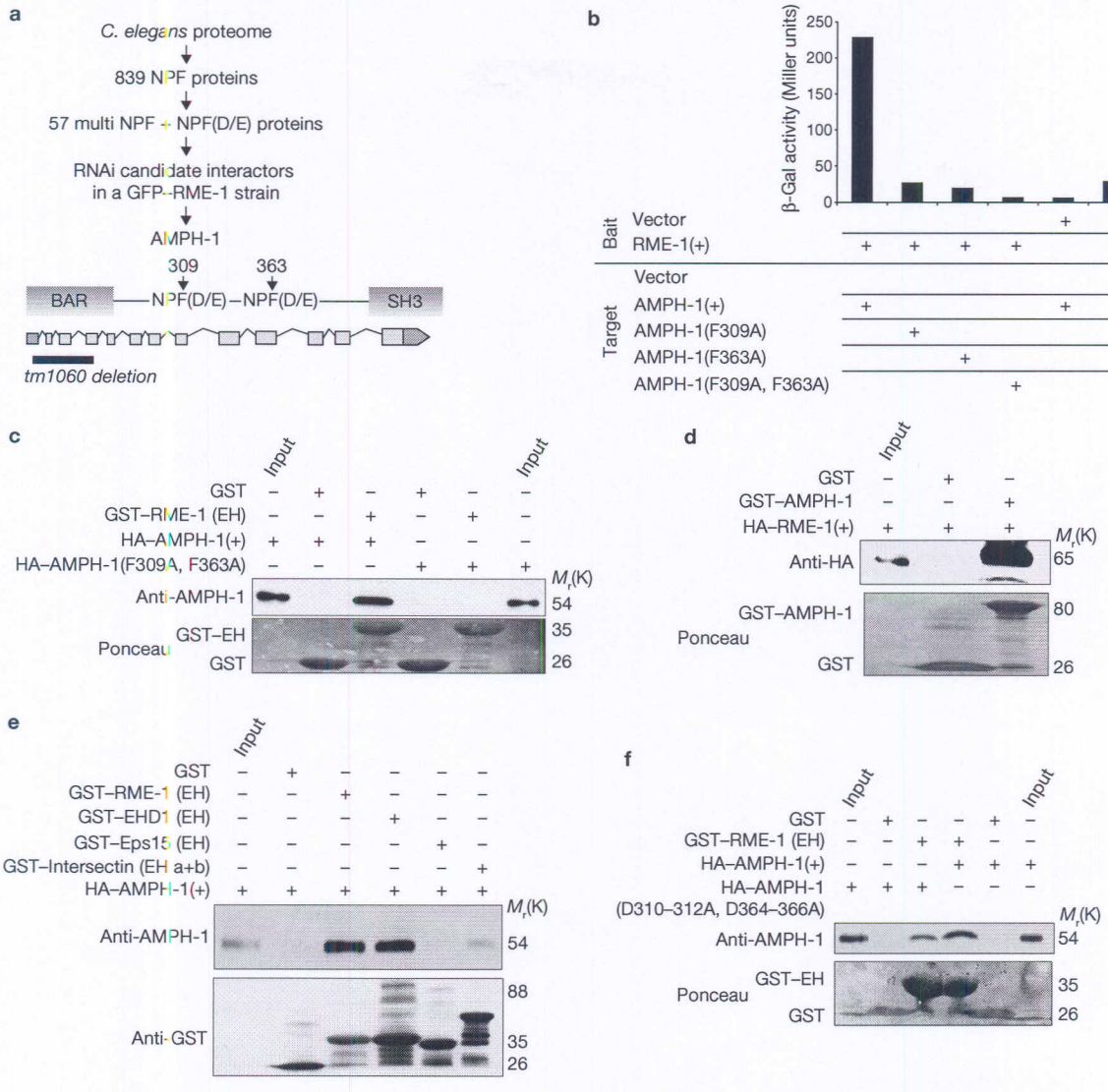

Figure 1 AMPH-1 physically interacts with RME-1. (**a**) A flowchart (top) showing the steps involved in identifying AMPH-1 as an RME-1 EH-domain-interacting protein. Bioinformatic searches of the *C. elegans* proteome identified multi-Asn-Pro-Phe (NPF)- and NPF(D/E)-containing candidates, which were assayed for effects on GFP–RME-1 subcellular localization after RNAi-mediated depletion, leading to the identification of AMPH-1, a BAR and SH3 domain-containing protein. A diagram of the *C. elegans amph-1* gene (bottom) indicating 5′ and 3′ untranslated regions (dark grey boxes), exons (light grey boxes), introns (connecting lines) and the location of the *amph-1(tm1060)* deletion. (**b**) RME-1 (residues 447–555) was expressed as bait in a yeast reporter strain. AMPH-1 (residues 230–394) and its mutant forms were expressed as prey in the same yeast cells. Interaction between bait and prey was assayed by quantitative β-galactosidase (β-Gal) assays (Supplementary Information, Table S1). Mutation of either Asn-Pro-Phe motif to Asn-Pro-Ala was sufficient to significantly disrupt the interaction. The *y*-axis represents β-Gal activity in Miller units. Data are from two independent experiments. (**c**) Glutathione beads loaded with recombinant GST or GST–RME-1 (442–576) were incubated with *in vitro*-expressed HA–AMPH-1(+) or HA–AMPH-1(F309A, F363A). A western blot for bound proteins was probed with an anti-AMPH-1 antibody. Input lanes contained 50% target protein. The lower panel shows equivalent loading of bait GST fusion proteins. (**d**) Glutathione beads loaded with recombinant GST or GST–AMPH-1 (full length) were incubated with *in vitro*-expressed HA–RME-1 (full length). Bound proteins were analysed by a western blot probed with an anti-HA antibody. Input lanes contain 10% of the target protein HA–RME-1. The lower panel shows equivalent loading of bait GST fusion proteins. (**e**) Glutathione beads loaded with recombinant GST, GST–RME- 1 (442–576), GST–mRme-1/EHD1 (EH domain), GST–Eps15 (EH domain 2) or GST–Intersectin (EH domains a + b) were incubated with *in vitro*-expressed target protein HA–AMPH-1(+). Bound proteins were analysed by western blotting with an anti-AMPH-1 antibody. Input lane contains 10% target protein. The lower panel shows equivalent loading of bait GST fusion proteins. (**f**) Glutathione beads loaded with recombinant GST or GST–RME-1 (442–576) were incubated with *in vitro*-expressed target proteins HA–AMPH-1(+) or HA–AMPH-1(D310–312A, D364–366A). Bound proteins were analysed by western blotting with an anti-AMPH-1 antibody. Input lanes contained 50% of the target protein. The lower panel shows equivalent loading of bait GST fusion proteins.

sequence (Fig.1a and Methods). Of these predicted proteins, 74 contained multiple Asn-Pro-Phe sequences and/or Asn-Pro-Phe sequences followed by acidic Asp/Glu stretches. To determine which of these 74 candidate RME-1 interactors might be physiologically relevant, we performed RNA interference (RNAi)-mediated knockdown of each candidate in transgenic animals expressing GFP-tagged RME-1. We reasoned that knockdown of a physiologically relevant RME-1 binding partner could alter RME-1 subcellular localization and/or recycling endosome morphology. Among the small number of candidate interactors whose RNAi-mediated knockdown affected RME-1 localization we noted AMPH-1, the only *C. elegans* member

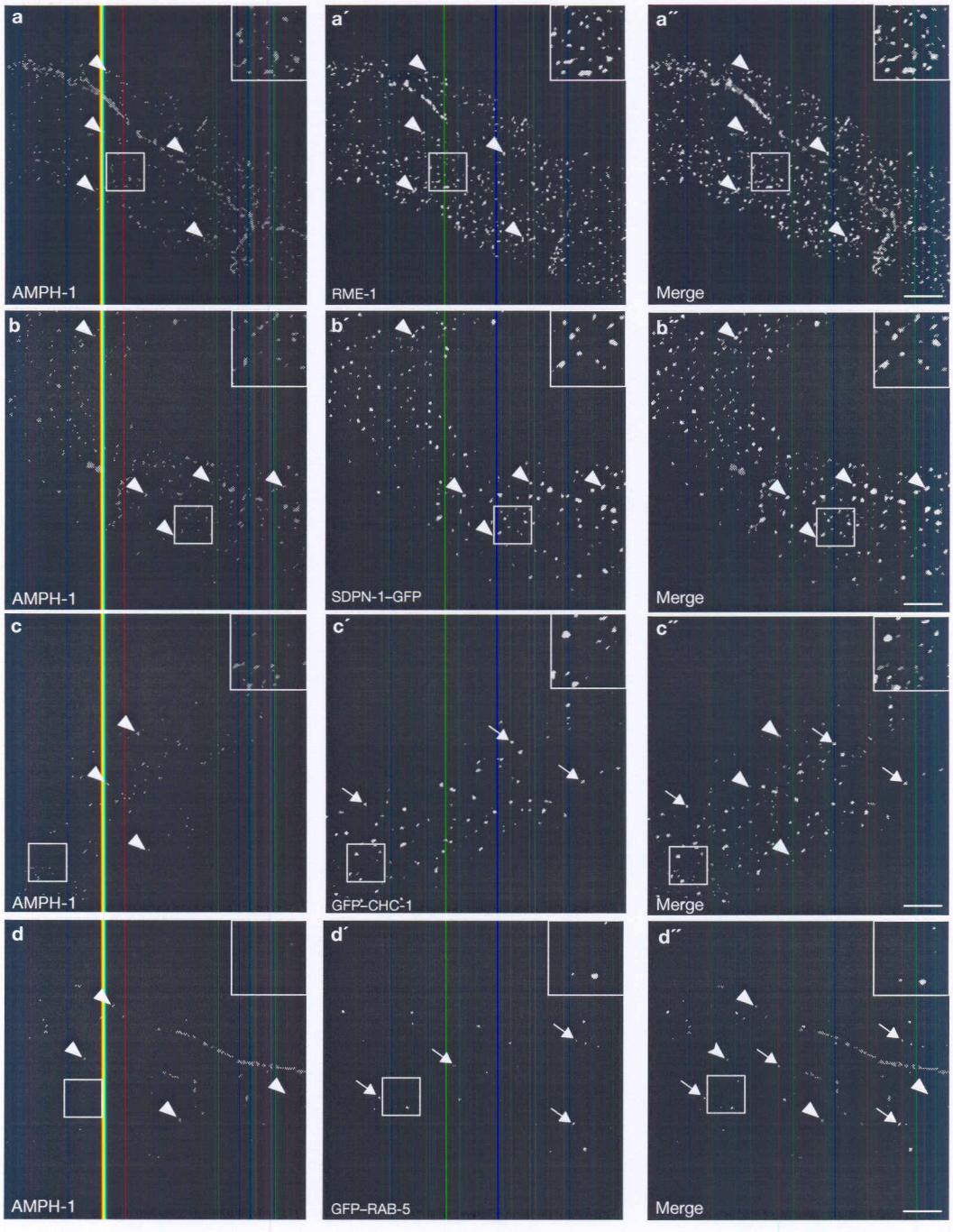

Figure 2 AMPH-1 co-localizes with RME-1 and SDPN-1 on recycling endosomes. Wild-type N2 worms or various GFP-labelled transgenic worms were synchronized and grown to the adult stage before decapitation by microsurgery. The extruded worm intestines were fixed and immunostained with antibodies for visualization of endogenous protein localization. (**a**–**a**′′) Endogenous AMPH-1 labelled with a rabbit polyclonal anti-AMPH-1 antibody (red) co-localizes extensively with endogenous RME-1 labelled with a mouse monoclonal antibody (green). Arrowheads indicate structures labelled by both AMPH-1 and RME-1. (**b**–**b**′′) Endogenous AMPH-1 (red) colocalizes significantly with the recycling endosome marker SDPN-1–GFP (green). Arrowheads indicate structures labelled by both AMPH-1 and SDPN-1. (**c**–**c**′′) Endogenous AMPH-1 (red) does not colocalize significantly with clathrin (GFP–CHC-1; green). Arrowheads indicate structures labelled by AMPH-1 and arrows indicate structures labelled by GFP–CHC-1. (**d**–**d**′′) Endogenous AMPH-1 (red) does not colocalize with the early endosome marker GFP–RAB-5 (green). Arrowheads indicate structures labelled by AMPH-1 and arrows indicate structures labelled by GFP–RAB-5. Scale bars, 10 μm.

of the Amphiphysin/BIN1 family of BAR- and SH3 (Src-homology domain 3) domain-containing proteins (Fig. 1a). This was especially intriguing given the known interactions of mammalian Amphiphysin with Dynamin in presynaptic membranes of the nervous system[15,16].

Physical interaction between RME-1 and AMPH-1

To determine whether AMPH-1 can physically bind to RME-1, we performed yeast two-hybrid based tests and GST pulldown analysis. AMPH-1 interacted with the RME-1 EH domain in the yeast two-hybrid

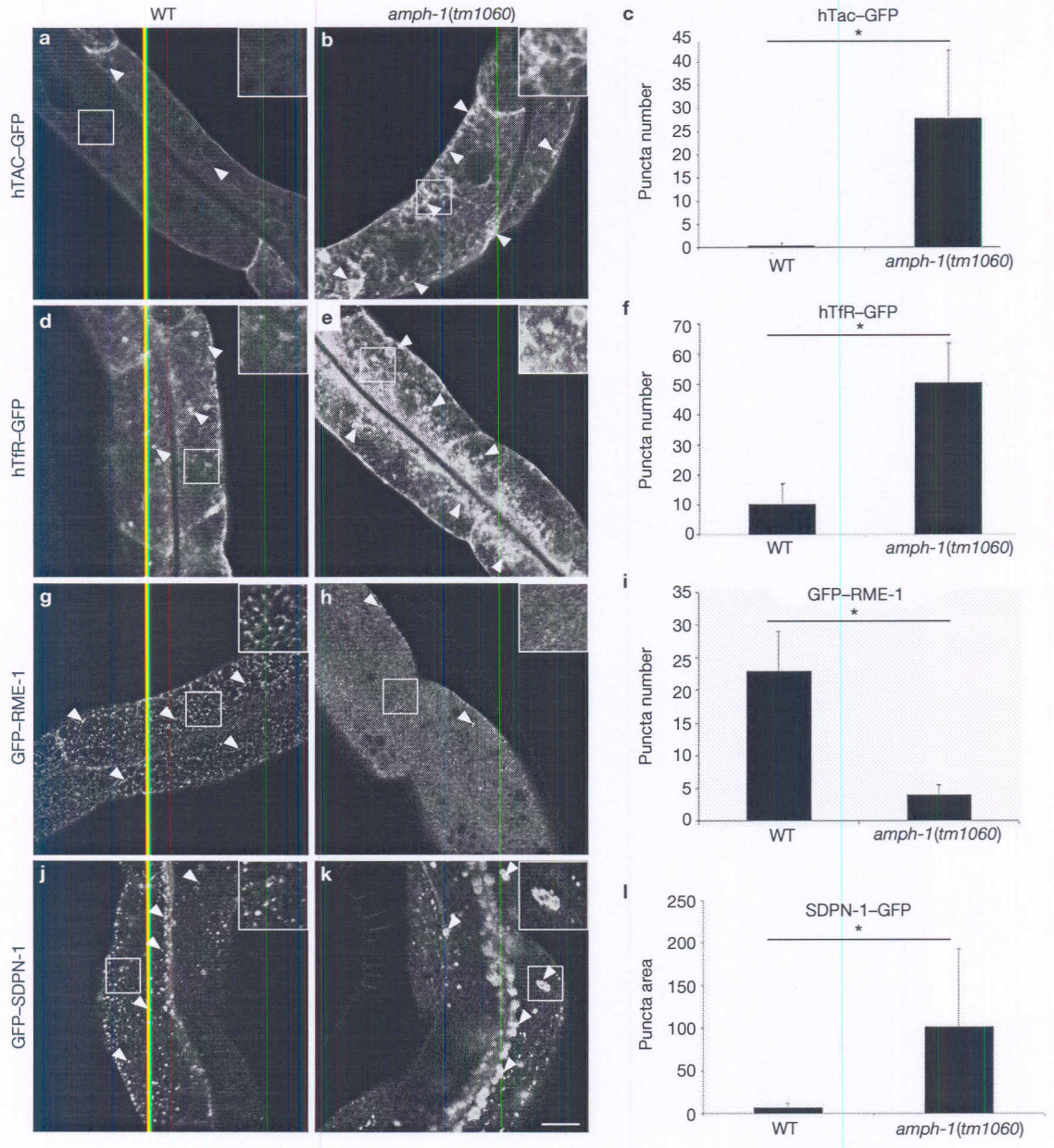

Figure 3 *C. elegans amph-1* mutants show abnormal trafficking of recycling cargo and morphologically abnormal recycling endosomes. (**a**–**c**) hTAC–GFP, a cargo protein internalized independently of clathrin, accumulates intracellularly in *amph-1* mutants. (**a**, **b**) Intestines of live intact animals showing hTAC–GFP localization in wild-type and *amph-1* mutant worms. (**c**) Quantification of hTAC–GFP signals as in **a** and **b** with respect to the average number of labelled structures per unit area. $*P = 1.2 \times 10^{-12}$. (**d**–**f**) hTfR–GFP, a clathrin-dependent cargo protein, accumulates intracellularly in *amph-1* mutants. (**d**, **e**) Intestines of live intact animals showing hTfR–GFP localization in wild-type and *amph-1* mutant worms. (**f**) Quantification of hTfR–GFP signals as in **d** and **e** with respect to the average number of labelled structures per unit area. $*P = 9.7 \times 10^{-22}$. Arrowheads in **a**–**e** indicate punctate and tubular signals. (**g**–**i**) Loss of GFP–RME-1 labelling of basolateral recycling endosomes in the *amph-1(tm1060)* mutants. (**g**, **h**) Confocal micrographs of intenstinally expressed GFP–RME-1 localization in wild-type and *amph-1* mutant worms. Arrowheads indicate GFP–RME-1 signal. (**i**) Quantification of GFP–RME-1 signals as in **g** and **h** with respect to average number of labelled structures per unit area. $*P = 1.1424 \times 10^{-7}$. (**j**–**l**) SDPN-1–GFP-labelled recycling endosomes are both reduced in number and appear larger in the *amph-1(tm1060)* mutant intestines (**k**) relative to those in wild-type intestines (**j**). Arrowheads indicate SDPN-1–GFP-labelled structures. (**l**) Quantification of SDPN-1–GFP signals as in **j** and **k** with respect to the average area of labelled structures. $*P = 2.4 \times 10^{-6}$. Data in **c**, **f**, **i** and **l** represent mean ± s.d. and $n = 30$ sampled fields (six animals of each genotype were sampled from five different regions their intestine). *P* values were determined using the one-tailed Student's *t*-test. Scale bar, 10 μm. WT, wild-type.

system (Fig. 1b). The interaction was abolished when either or both AMPH-1 Asn-Pro-Phe sequences were altered by substituting alanine for Phe 309 and/or Phe 363 (Fig. 1b). In the pulldown experiment, full-length AMPH-1 from wild-type worm lysates or *in vitro*-translated AMPH-1(+) was efficiently isolated by immobilized GST–RME-1 EH-domain fusion protein (Fig. 1c; Supplementary Information, Fig. S1b). AMPH-1 also bound strongly to the EH-domain of mammalian mRme-1/EHD1 in this assay (Fig. 1e). Little or no binding of AMPH-1 to the EH-domains of other endocytic proteins, Eps15 or Intersectin, was observed, indicating the specificity of the interaction (Fig. 1e). Furthermore, *in vitro*-translated

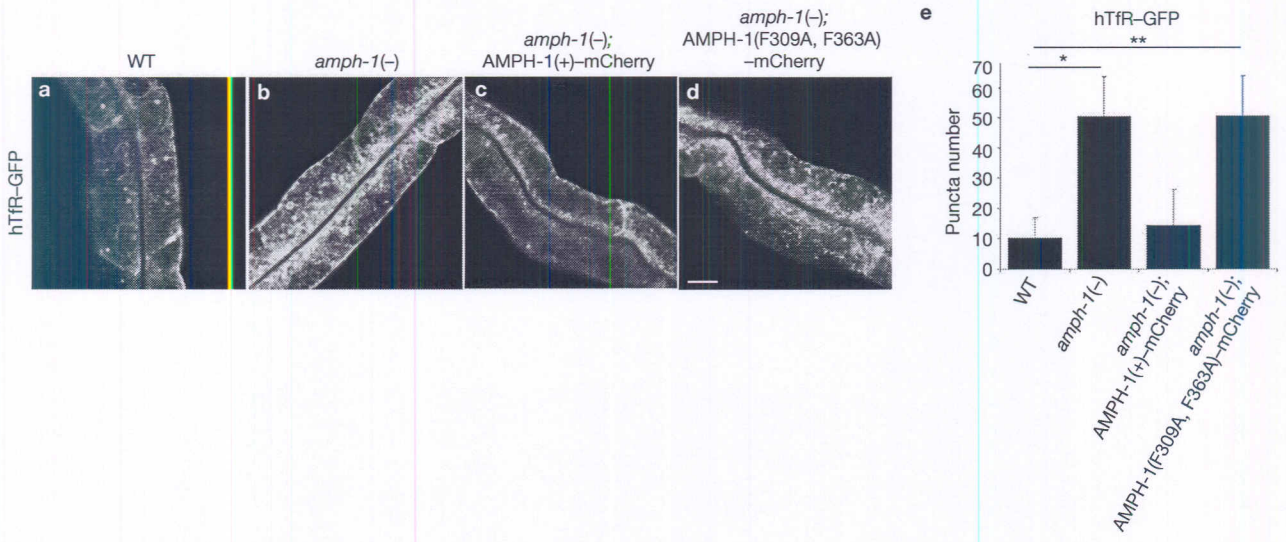

Figure 4 AMPH-1 function in endocytic recycling requires interaction with RME-1. (**a**–**e**) AMPH-1(+) and the interaction-deficient AMPH-1(F309A, F363A) mutant were expressed as mCherry fusion proteins in *amph-1*(*tm1060*) mutant intestines. Synchronized adult worms were imaged by confocal microscopy (**a**–**d**). AMPH-1(+) (**c**), but not AMPH-1(F309A, F363A) (**d**), could rescue the abnormal accumulation of recycling cargo hTfR–GFP in *amph-1*(*tm1060*) mutants. (**e**) Quantification of the hTfR–GFP-labelled structures in the worms with respect to average number of labelled structures per unit area. $*P = 9.7 \times 10^{-22}$, $**P = 9.4 \times 10^{-22}$ (one-tailed Student's *t*-test). Data are mean ± s.d., $n = 30$ sampled fields (six animals of each genotype sampled from five different regions of their intestine). Scale bar, 10 μm.

AMPH-1(F309A, F363A), which lacks intact Asn-Pro-Phe motifs, failed to bind to the GST–RME-1 EH-domain fusion protein (Fig. 1c), and alanine substitution for the first three aspartic acid residues following each Asn-Pro-Phe motif reduced binding (Fig. 1f). Full-length *in vitro*-translated RME-1 could be isolated by immobilized full-length GST–AMPH-1 fusion protein (Fig.1d). We conclude that AMPH-1 binds directly to RME-1, and that this interaction requires the RME-1 EH domain and the two Asn-Pro-Phe(Asp/Glu) motifs present within AMPH-1.

AMPH-1 is enriched on recycling endosomes

RME-1 is ubiquitously expressed in *C. elegans*, and is highly enriched on tubulo-vesicular basolateral recycling endosomes in the polarized intestinal epithelium[1]. In transgenic animals, AMPH-1–GFP under the control of *amph-1* genomic DNA regulatory sequences was similarly widely expressed (Supplementary Information, Fig. S1c–j). Affinity-purified anti-AMPH-1 antibodies detected a single band of the expected size for AMPH-1 in western blots of wild-type worms. This band was absent in *amph-1*(*tm1060*) deletion-mutant worms (Supplementary Information, Fig. S1a), establishing the specificity of the antibody.

Using immunofluorescence, we found that endogenous AMPH-1 colocalizes extensively with endogenous RME-1 on tubulovesicular basolateral recycling endosomes (Fig. 2a–a′′), and on more weakly labelled sub-apical structures of the worm intestine, possibly the apical recycling endosomes (Supplementary Information, Fig. S2c–c′′). Although there was significant overlap of RME-1 and AMPH-1 labelling on the recycling endosome, the two proteins did not label the endosome identically. This may reflect differences in the degree of association with specific endosomal subdomains, or temporal differences in the assembly or disassembly kinetics of the two proteins. Endogenous AMPH-1 also colocalized with basolateral GFP-tagged SDPN-1 (a *C. elegans* homologue of synaptic dynamin binding protein, also known as pacsin), another marker for the *C. elegans* recycling endosome (Fig. 2b–b′′)[17]. Anti-AMPH-1 staining failed to colocalize with markers for clathrin-coated pits (GFP-tagged CHC-1/clathrin)[18], early endosomes (GFP–RAB-5; ref. 19), late endosomes (GFP–RAB-7; ref. 19) or the Golgi (mannosidase–GFP)[19], indicating that AMPH-1 is specifically enriched on recycling endosomes (Fig. 2c–c′′, d–d′′; Supplementary Information, Fig. S3). We also observed extensive colocalization of mCherry–RME-1 and AMPH-1–GFP in living transgenic animals, supporting the data derived from fixed tissue (Supplementary Information, Fig. S2a–a′′).

The lack of AMPH-1 association with clathrin-coated pits is consistent with the absence of a consensus CLAP (clathrin and AP2 adaptor binding) domain in *C. elegans* AMPH-1. In fact, the CLAP domain is specific to certain isoforms of vertebrate Amphiphysins and is not found in any known invertebrate Amphiphysin family member[20]. In *Drosophila melanogaster*, dAmph has been shown to lack Dynamin (encoded by *Shibire*)-binding ability, does not colocalize with *Shibire*/Dynamin, and does not produce shibire-like phenotypes when mutated[21–23]. While *Drosophila Shibire*/Dynamin and *C. elegans* Dynamin (also known as DYN-1) do possess proline-rich sequences, neither Dynamin orthologue contains the Pro-X-Arg-Pro-X-Arg consensus motif that is recognized by Amphiphysin SH3 domains in vertebrates[24]. Notably, *Drosophila* Amphiphysin does contain an Asn-Pro-Phe sequence followed by acidic residues, suggesting potential interaction with an RME-1/EHD family member.

amph-1-null mutants are defective in endocytic recycling

To determine the function of AMPH-1 *in vivo*, we characterized the phenotype of *amph-1*(*tm1060*)-null mutants. To detect recycling defects, we first focused on the previously validated model recycling cargo proteins hTfR–GFP (human transferrin receptor) and hTac–GFP (IL2-receptor alpha chain)[25,26]. hTfR is internalized through clathrin-dependent mechanisms, and hTac is internalized by clathrin-independent mechanisms[27]. Both of these model recycling cargo proteins depend on RME-1/EHD1

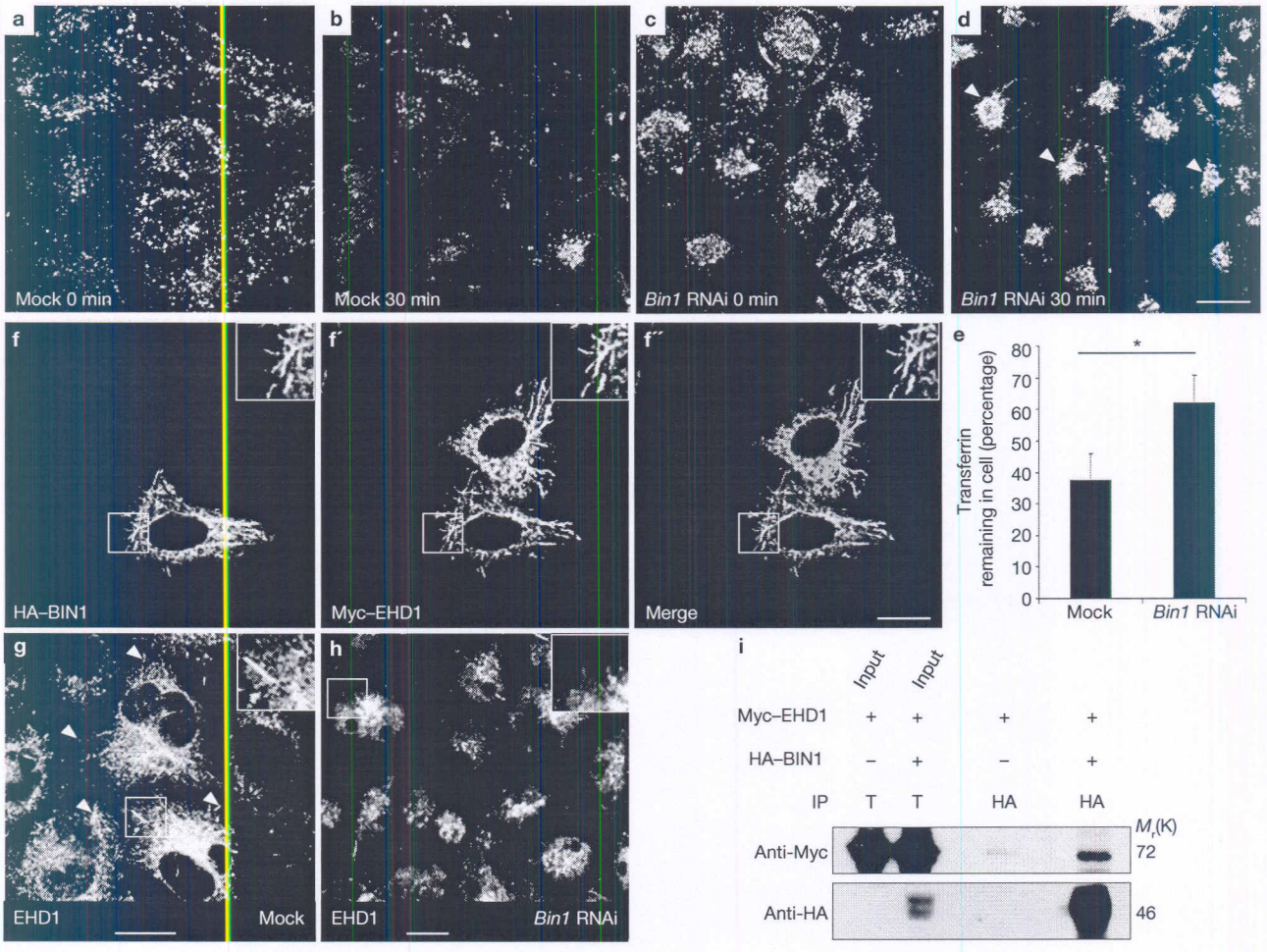

Figure 5 RNAi-mediated depletion of human Bin1 impairs transferrin recycling and disrupts mRme-1/EHD1-positive recycling endosome tubules. (**a**–**d**) Representative fields are shown for mock-treated HeLa cells or HeLa cells subjected to *Bin1* RNAi after 5 min of Alexa-488 transferrin uptake (**a**, **c**) and 30 min chase in complete medium (recycling; **b**, **d**). (**e**) The average cell fluorescence was determined from confocal micrographs of 80 HeLa cells, mock-treated or subjected to *Bin1* RNAi, after Alexa-488 transferrin uptake followed by 30 min chase (Supplementary Information, Table S2). Data are mean ± s.e.m. from three independent experiments, $n = 80$ cells per experimental condition. $P = 1.06 \times 10^{-35}$ (one-tailed Student's *t*-test). (**f**–**f**″) BIN1 and mRme-1/EHD1 colocalize on intracellular tubules. HeLa cells transfected with 2×HA–BIN1 isoform 10 and Myc–EHD1 were visualized by confocal microscopy after immunostaining with primary antibodies, mouse anti-HA (**f**) and rabbit anti-EHD1 (**f**′), followed by staining with appropriate fluorochrome-labelled secondary antibodies. The insets and merged image in **f**″ demonstrate colocalization of HA–BIN1 isoform 10 with Myc–EHD1-positive tubules. (**g**, **h**) mRme-1/EHD1-positive tubules are disrupted by Bin1-depletion. HeLa cells grown on coverslips were mock-treated or subjected to *Bin1* RNAi. Endogenous EHD1 was visualized by confocal microscopy after immunostaining with an affinity-purified polyclonal rabbit anti-EHD1 antibody, followed by staining with Alexa Fluor 488 anti-rabbit secondary antibodies. Note the loss of tubular EHD1 labelling after Bin1 depletion. (**i**) mRme-1/EHD1 physically associates with BIN1 isoform 10. HeLa cells were transfected with Myc–EHD1 or co-transfected with Myc–EHD1 and 2×HA–BIN1 isoform 10. Cells were lysed and lysates were immunoprecipitated with goat anti-HA antibody-conjugated agarose beads. Unbound protein was removed by successive washes. Bound proteins were eluted with Laemmli sample buffer, separated by SDS–PAGE, and analysed by western blotting with an anti-Myc antibody. Input lane contains 1% of the lysate used in the binding assay. T denotes total lysate. Scale bars, 10 μm.

for their recycling in mammalian and worm cells, accumulating in recycling endosomes in the absence of RME-1/EHD1 function[2,3,17,19]. The number of hTac–GFP and hTfR–GFP intracellular puncta in *amph-1* mutants increased by more than 10-fold, compared with those in wild-type control worms (Fig. 3a–f). These results indicate a defect in basolateral recycling in the intestinal epithelia of *amph-1* mutants that is very similar to that found in *rme-1* mutants.

Specific disruption of recycling endosomes in *amph-1* mutants

Further analysis showed that RME-1 labelling of basolateral recycling endosomes was profoundly abnormal in *amph-1*-mutant animals, with loss of most tubular labelling and an increase in diffuse GFP–RME-1 labelling. Only a small number of GFP–RME-1-labelled punctate structures remained (Fig. 3g–i; Supplementary Information, Fig. S5). The loss of RME-1 from recycling endosomes confirmed the *amph-1* (RNAi) results from the initial screen, suggesting that AMPH-1 functions, at least in part, in recruiting RME-1 to the recycling endosome membrane. We also found that loss of *amph-1* disrupted another recycling endosome marker SDPN-1–GFP, causing greatly reduced SDPN-1–GFP puncta number and gross enlargement of remaining labelled structures (Fig. 3j–l). This phenotype was very similar to one we found previously in *rme-1* mutants[17], further indicating that AMPH-1 functions

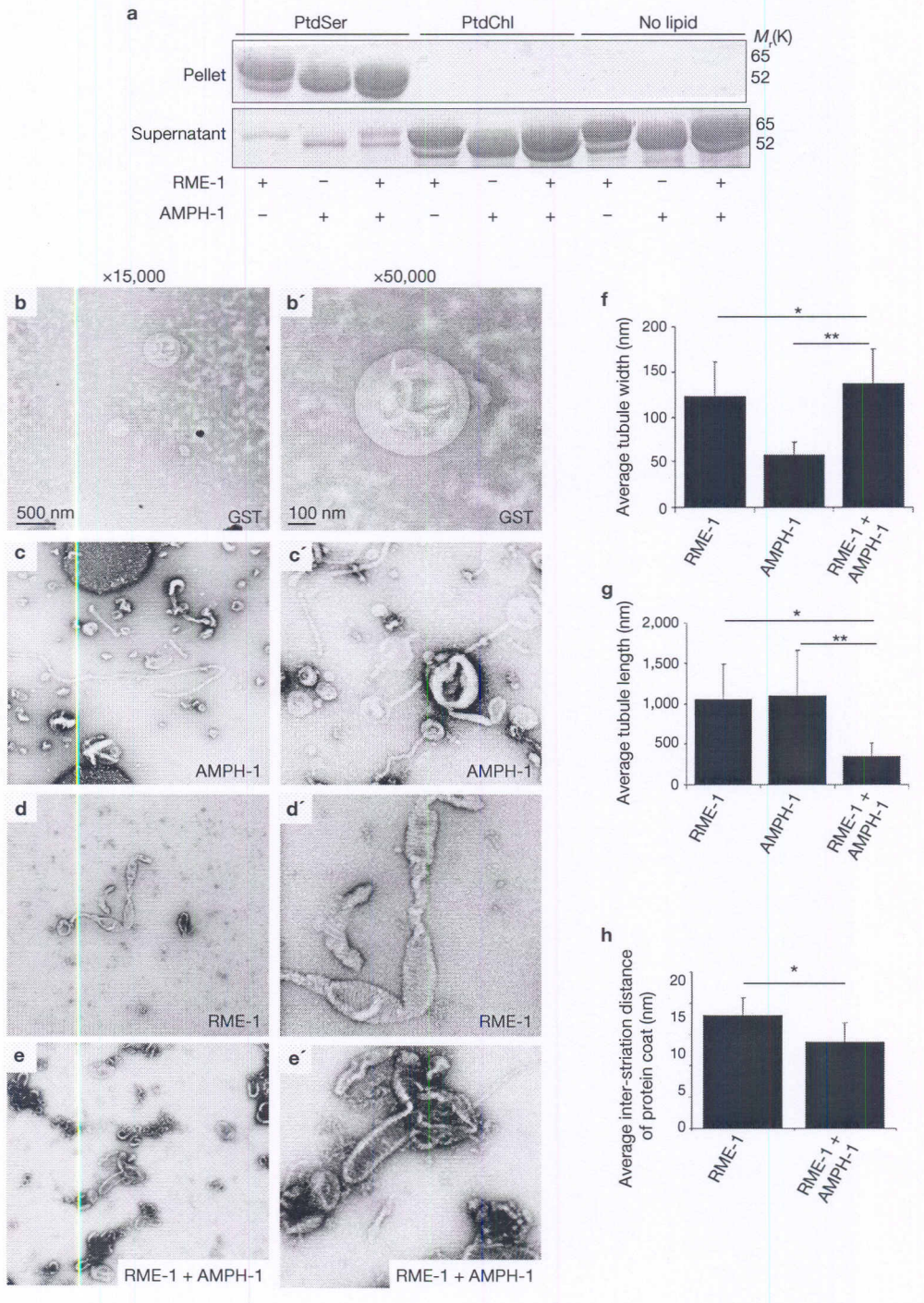

Figure 6 Membrane binding and tubulation by AMPH-1 and RME-1 *in vitro*. (**a**) Coomassie-stained gels of supernatant and pellet fractions from liposome co-sedimentation assays are shown. Binding reactions were performed in the absence or presence of 100% phosphatidylserine (PtdSer), or 100% phosphatidylcholine (PtdChl) liposomes (0.33 mg ml^{-1}, average diameter 0.4 μm). Liposomes were incubated with 1 mM of ATP-γ-S and 1 μM of full-length AMPH-1 or RME-1 protein, or equimolar quantities of both proteins, as indicated. (**b**–**e**′) Electron micrographs of negatively stained PtdSer liposomes, prepared as above (but used at 0.05 mg ml^{-1}) in the presence of 1 mM of ATP-γ-S and 2.5 μM of GST (**b**, **b**′), AMPH-1 (**c**–**c**′) or RME-1 (**d**, **d**′), or equimolar quantities of AMPH-1 and RME-1 (**e**, **e**′). (**f**) Quantification of tubule widths. For each experimental condition, the width was measured for every tubule on 15 electron micrographs. For tubules with uneven width, the average width measurement from several representative points along the tubule was calculated. Error bars represent mean ± s.d., $n = 15$ representative tubules per experimental condition. $^{*}P = 0.0074$, $^{**}P = 1.29 \times 10^{-13}$. (**g**) Quantification of tubule lengths. The length from the edge of the liposome body to end of the tubule was measured for every tubule on 15 electron micrographs per experimental condition. Error bars represent mean ± s.d., $n = 15$ representative tubules per experimental condition. $^{*}P = 1.7 \times 10^{-7}$, $^{**}P = 3.2 \times 10^{-4}$. (**h**) Quantification of inter-striation distance. Error bars represent mean ± s.d., $n = 15$ representative tubules per experimental condition. The average distance between every successive ring-like striation was calculated for each condition. $^{*}P = 0.0031$. *P* values were determined using the one-tailed Student's *t*-test. Full scans of blots in **a** can be seen in Supplementary Information, Fig. S8a, b.

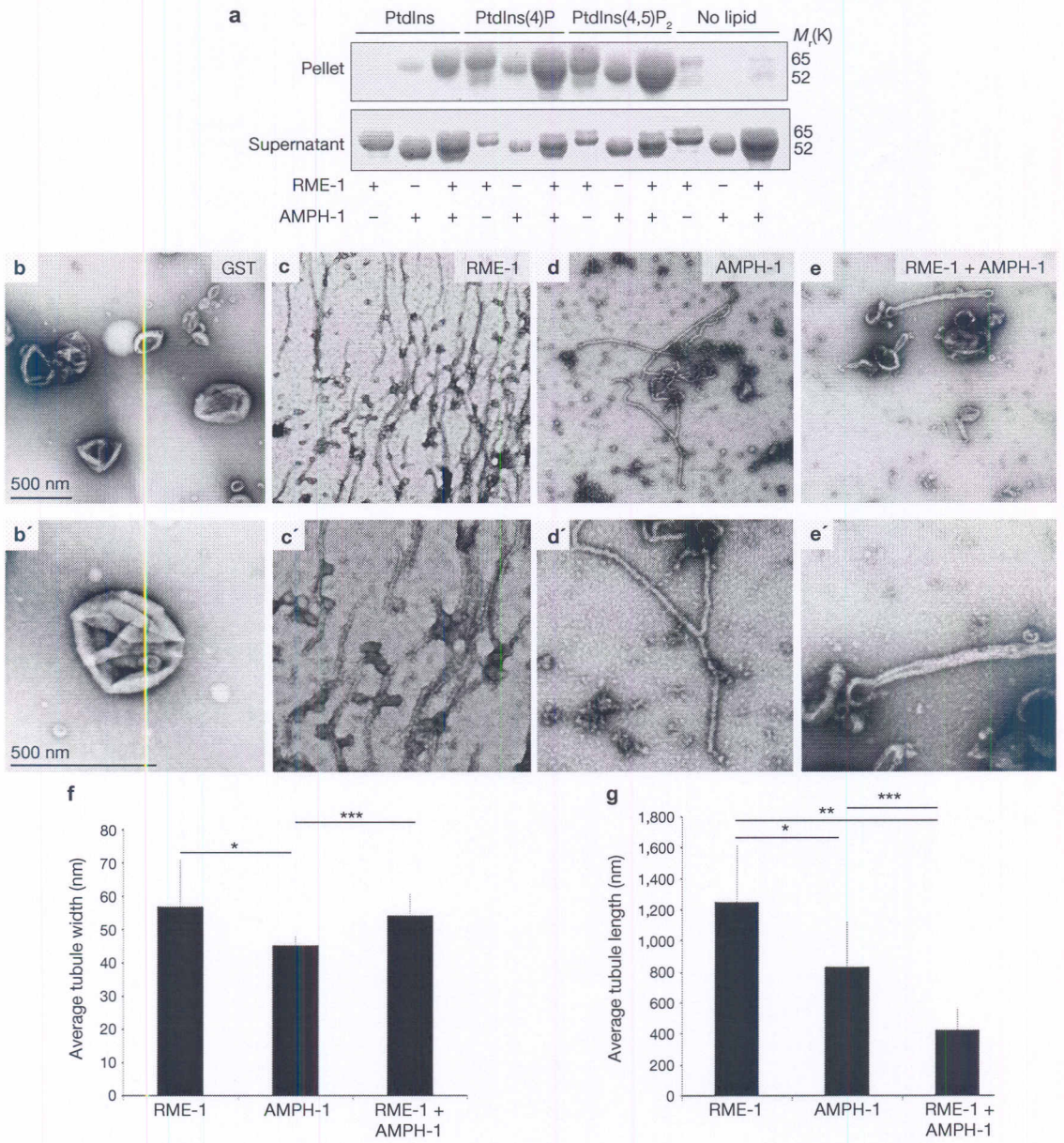

Figure 7 *In vitro* membrane binding and tubulation by AMPH-1 and RME-1 to PtdIns-containing liposomes. (**a**) Coomassie-stained gels of supernatant and pellet fractions from liposome co-sedimentation assays are shown. Binding reactions were performed in the absence or presence of liposomes (0.33 mg ml^{-1}, 4 μm average diameter) containing 80% phosphatidylcholine (PtdChl), 10% phosphatidylserine (PtdSer) and 10% of unphosphorylated PtdIns, (PtdIns(4)P) or PtdIns(4,5)P_2. Liposomes were incubated with 1 mM of ATP-γ-S and 1 μM of full-length AMPH-1, RME-1 or equimolar quantities of both proteins, as indicated. (**b**-**e**′) Electron micrographs of negatively stained PtdIns(4,5)P_2 liposomes, prepared as above, (but used at 0.05 mg ml^{-1}), in the presence of 1 mM of ATP-γ-S and 2.5 μM of GST (**b**, **b**′), RME-1-1 (**c**, **c**′), AMPH-1 (**d**, **d**′) or equimolar quantities of AMPH-1 and RME-1 (**e**, **e**′). Images in **b**–**e** are at ×50,000 magnification, and images in **b**′–**e**′ are enlarged regions from panels **b**–**e**. (**f**) Quantification of tubule widths. For each experimental condition, the width was measured for every tubule on 10 electron micrographs. For tubules with uneven width, the average measurement from several representative points along the tubule was calculated. Error bars represent mean ± s.d., $n = 10$ representative tubules. The asterisk indicates a significant difference in the one-tailed Student's T-test: $*P = 0.01$, $***P = 0.004$. (**g**) Quantification of tubule lengths. The length from the edge of the liposome body to end of the tubule was measured for every tubule on 10 electron micrographs per experimental condition. Error bars represent mean ± s.d., $n = 10$ representative tubules for each condition. $*P = 0.005$, $**P = 1.8 \times 10^{-6}$, $***P = 3.8 \times 10^{-4}$. *P* values were determined using the one-tailed Student's *t*-test. Full scans of blots in **a** can be seen in Supplementary Information, Fig. S8c d.

with RME-1 *in vivo*. We noted, however, that some *amph-1* phenotypes seemed weaker than *rme-1* phenotypes, such as in the accumulation of fluid-filled vacuoles in the intestine, and in the transport of yolk proteins from the intestine to the oocyte (data not shown). This might indicate some functional redundancy between AMPH-1 and other BAR-domain adaptor proteins, or residual RME-1 activity in the absence of AMPH-1.

We also examined *amph-1* mutants for effects on early endosomes. This was particularly important because mutants known to affect an earlier recycling step, from the early endosome to the recycling

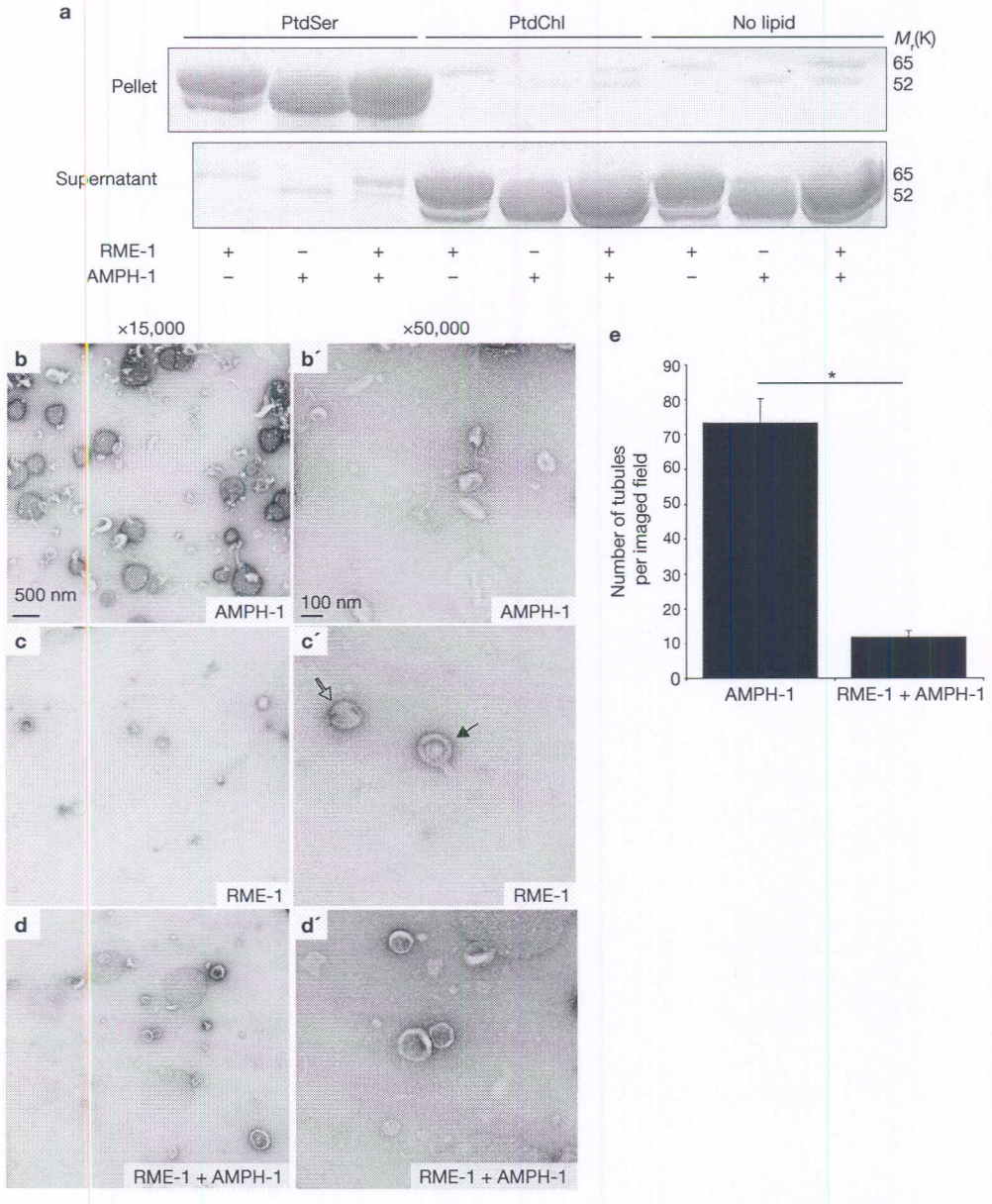

Figure 8 Nucleotide effects on RME-1- and AMPH-1-mediated liposome tubulation. (**a**) Coomassie-stained gels of supernatant and pellet fractions from liposome co-sedimentation assays are shown. Binding reactions were performed in the absence or presence liposomes (0.33 mg ml^{-1}, 4 μm average diameter) containing 100% phosphatidylserine (PtdSer), or 100% phosphatidylcholine (PtdChl). Liposomes were incubated with ADP (1 mM) and 1 μM of full-length AMPH-1 or RME-1 protein, or equimolar quantities of both proteins, as indicated. Note that RME-1 can bind to PtdSer liposomes in the presence of ADP. Tubulation experiments were performed with each protein (2.5 μM) and ADP (1 mM) incubated with 100% PtdSer liposomes (0.05mg ml^{-1}). (**b**, **b**′) AMPH-1 incubated with PtdSer liposomes in the presence of ADP (compare with ATP-γ-S in Fig. 5 c, c′). (**c**, **c**′) RME-1 incubated with PtdSer liposomes in the presence of ADP (compare with ATP-γ-S in Fig. 5 d, d′). RME-1 (ADP) lacks tubulation capacity and most liposomes remain spherical (open arrow) in the presence of RME-1 (ADP). Striations are often visible and rare short protrusions (closed arrow) are present on occasional liposomes. (**d**, **d**′) RME-1 in its ADP-bound state can affect the tubulation ability of AMPH-1 as observed in an experiment containing equimolar concentrations of both proteins in the presence of ADP. (**e**) Quantification reveals an approximately 7-fold decrease in the number of tubules in conditions where RME-1 (ADP) is present with AMPH-1, as compared to tubulation produced by AMPH-1 alone. Error bars represent mean ± s.d., $n = 10$ representative fields for each condition (imaged at ×3,000 magnification), $^*P = 1.48 \times 10^{-15}$ (one-tailed Student's *t*-test). Full scans of blots in **a** can be seen in Supplementary Information, Fig. S8e, f.

endosome, produce a similar set of phenotypes, including loss of RME-1-labelled recycling endosomes and intracellular trapping of recycling cargo proteins, such as hTac–GFP[19]. The key distinguishing characteristic of an earlier block, such as that shown by *rab-10* mutants, is the dramatic over-accumulation of early endosomes, a phenotype not found in *rme-1* mutants[19]. Consistent with a later function for AMPH-1 at the recycling endosome to plasma membrane step, the morphology and distribution of early-endosome markers GFP–RAB-5 and GFP–RAB-10 was unperturbed in *amph-1* mutants (Supplementary Information, Fig. S4a–f).

Finally, because mammalian amphiphysin has been associated with plasma membrane clathrin-coated pits[16,28–30], we investigated whether *amph-1* mutants alter the morphology or distribution of functional GFP-tagged Dynamin or clathrin. We found that DYN-1–GFP and GFP–CHC-1 localization was unaltered in *amph-1* mutants, consistent with the proposal that *C. elegans* AMPH-1 does not interact with Dynamin, and similar to previous findings in *Drosophila* (Supplementary Information, Fig. S4g–l)[21–23]. Thus, we did not find any evidence that worm AMPH-1 is involved in recruiting DYN-1/Dynamin to the clathrin-coated pit during endocytic uptake at the plasma membrane. Instead, *C. elegans* AMPH-1 seems to be specific for RME-1-mediated recycling processes.

AMPH-1 requires interaction with RME-1 for recycling function

Having established the effects of AMPH-1 loss on endocytic traffic, and the close association of AMPH-1 with RME-1, we sought to determine the importance of the AMPH-1–RME-1 physical association *in vivo*. Thus, we tested the ability of transgenically expressed AMPH-1, with or without intact RME-1-interaction motifs, to rescue *amph-1* mutant phenotypes. We found that although AMPH-1(F309A, F363A) was expressed as efficiently as AMPH-1(+) (Supplementary Information Fig. S5a–b), only AMPH-1(+) rescued the *amph-1* mutant phenotypes with respect to hTfR accumulation and RME-1 localization (Fig. 4; Supplementary Information, Fig. S5c–g), indicating that AMPH-1 requires interaction with RME-1 to perform its role as an endocytic recycling regulator. We also found that AMPH-1 protein is mislocalized in *rme-1(0)* mutants. Instead of an extended tubulovesicular pattern, we observed a more concentrated localization of endogenous AMPH-1 to enlarged structures, similar to the abnormal localization of SDPN-1 in *rme-1* mutants (Supplementary Information, Fig. S5h–l). However, AMPH-1 still appeared to be associated with the membrane in the absence of RME-1, suggesting that AMPH-1 does not require RME-1 for membrane recruitment.

Mammalian BIN1/Amph2 functions in recycling

Unlike *C. elegans*, which seems to express only one Amphiphysin isoform, the mammalian genome contains two distinct Amphiphysin genes denoted *Amphiphysin 1* and *Amphiphysin 2* (also known as *Bin1*). Each of these genes encodes several protein isoforms. Amph1 is brain-specific and Amph2a is brain-enriched. Both of these isoforms contain a CLAP domain for clathrin and AP2 adaptor binding. Amph1 and Amph2a form heterodimers and are thought to aid endocytic uptake at the synaptic clathrin-coated pit, at least in part through interaction with Dynamin[15,16,28,29,31–33]. Other forms of Amph2 (also known as BIN1) lack clathrin–AP2 interaction modules. One specific isoform functions in muscle development[34], whereas other isoforms, such as BIN1 isoform 10, have no known function. In fact, it has been shown that Amph2-knockout MEF cells are not defective in endocytic uptake of transferrin, rather they show an approximate twofold increase in transferrin uptake[35].

Although the known BIN1 isoforms lack Asn-Pro-Phe sequences, and so may not bind to mammalian RME-1/EHD proteins directly, we considered the possibility that, similar to AMPH-1 in *C. elegans*, mammalian Amph2 might have a role in endocytic recycling. In fact, we observed weak co-immunoprecipitation of Myc–EHD1 with HA–BIN1 isoform 10 in transfected cells (Fig. 5i). As a direct measure of the importance of BIN1 in endocytic transport, we followed fluorescently labelled transferrin transport in BIN1-depleted HeLa cells using previously described pulse-chase assays[27]. BIN1-knockdown strongly reduced expression of all forms of Amph2 in HeLa cells as determined by western blotting (Supplementary Information, Fig. S6a). Consistent with the previously published results from knockout MEFs, we found that HeLa cells depleted of Amph2 are not defective in transferrin uptake. Rather, uptake was increased in BIN1-knockdown cells after 7 min of transferrin uptake as measured using FACS (fluorescence-activated cell sorting; mock-treated 348 ± 118 a.u., *Bin1* RNAi 662 ± 325 a.u., averaged from three independent experiments) or visualized by microscopy (Fig. 5a, c). Consistent with a role for BIN1 in recycling from the endocytic recycling compartment, we found that transferrin accumulated in the juxtanuclear compartment in Amph2-depleted cells (Fig. 5b, d), and recycling was delayed as measured by image quantification (Fig. 5e) as well as by FACS analysis (Supplementary Information, Fig. S6b).

Consistent with the idea that BIN1/Amph2 functions directly in transport from the endocytic recycling department, we found that BIN1 was enriched on distinctive mRME-1/EHD1-positive tubules. This could be visualized in cells overexpressing Myc–EHD1 and HA–BIN1 isoform 10 (Fig.5 f–f′′), and in untransfected cells showing the endogenous proteins using anti-EHD1 and anti-BIN1 (isoform non-specific) antibodies (Supplementary Information, Fig. S6c–c′′). The EHD1-positive tubules have been shown previously to be endogenous features of HeLa cells, emanating from the endocytic recycling compartment[3]. These tubular endosomes are involved in the recycling of cargo proteins from the endocytic recycling compartment to the plasma membrane[3], and the absence of EHD1 from these structures leads to impaired recycling[36]. We found that depletion of BIN1/Amph2 disrupted the EHD1-positive recycling tubules (Fig. 5g, h). After depletion of BIN1/Amph2, EHD1 localization was limited to a compact juxtanuclear localization, consistent with the main body of the endocytic recycling compartment (Fig. 5h)[37]. Taken together, these results indicate that BIN1/Amph2 is important for the formation and/or maintenance of endocytic recycling compartment-derived tubules. Furthermore, these results indicate that the requirement for an amphiphysin family protein in the endocytic recycling pathway is an evolutionarily conserved feature from worms to mammals.

Reconstitution of RME-1–AMPH-1 interactions in a liposome system

Previous reports have shown that mammalian Amphiphysin[38], mammalian Dynamin[15,33,38], and mammalian EHD2 (ref. 9) have the capacity to bind to negatively charged liposomes and to deform the membrane to produce tubules[15,38,9]. In mammalian HeLa cells, recycling endosomes are enriched in PtdIns(4,5)P_2 (phosphatidylinositol-4,5-bisphosphate) due to the activation of PI(5)K by Arf6 on these endosomes[39] and PtdIns(4)P (phosphatidylinositol-4-phosphate) has also been recently identified as a component of these endosomes[36]. As a first step towards determining the membrane-binding capacity of worm RME-1 and AMPH-1, we tested the interaction of purified recombinant RME-1 and AMPH-1 with liposomes in a sedimentation assay. We found that both RME-1 and AMPH-1 pelleted with acidic phosphatidylserine (PtdSer) liposomes, or with a more physiological liposome composition containing 10% PtdSer and 10% PtdIns, PtdIns(4,5)P_2 or PtdIns(4)P (Figs 6a, 7a). Interestingly, the binding to PtdIns(4,5)P_2 -, PtdIns(4)P- and PtdIns-containing liposomes seemed enhanced when both proteins were added to the reaction, compared with adding the proteins individually (Fig. 7a). We did not observe binding of either RME-1 or AMPH-1 to neutral phosphatidylcholine (PtdChl) liposomes (Figs 6a, 7a).

We observed equivalent binding of RME-1 to PtdSer liposomes in the presence of ADP or the non-hydrolysable ATP analogue ATP-γ-S, indicating that, under these binding conditions, RME-1 association with liposomes was independent of its nucleotide state (Figs 6a, 8a).

We also examined the morphology of liposomes incubated with RME-1 and/or AMPH-1 using electron microscopy. In the presence of ATP-γ-S, RME-1 tubulates PtdSer liposomes, with an average diameter of 400 nm, into approximately 120-nm wide tubules with an average length of 1 μm (Fig. 6d, d′, f, g). The tubules were decorated with ring-like striations reminiscent of structures formed by mammalian Dynamin and EHD2 on liposomes. The rings probably represent highly ordered RME-1 (ATP-γ-S) oligomers wrapped around the tubules, with regions of close and looser ring packing. We found that in the presence of ATPγS, RME-1 tubulated PtdIns(4,5)P_2, PtdSer and PtdChl-containing liposomes into longer, but narrower, tubules than those produced from liposomes containing only PtdSer (compare Fig. 6d, d′, f, g with Fig. 7c, c′, f, g). In profile, these tubules had an irregular spike-like, coated appearance. Frequently, we also observed structures resembling constrictions along the length of the tubule, imparting a beads-on-a-string appearance to the tubulating liposomes.

In the absence of RME-1, AMPH-1 tubulated PtdSer-containing liposomes, with an average diameter of 400 nm, into 50-nm wide tubules with an average length of 1.1 μm (Fig. 6c, c′, f, g), which was much narrower than the tubules formed in the presence of RME-1 alone. Similar results were obtained for AMPH-1 incubated with PtdIns(4,5)P_2, PtdSer and PtdChl-containing liposomes (Fig. 7d, d′).

The physical and functional interactions of AMPH-1 and RME-1 suggested that the two proteins work together to promote recycling through endosomal tubules. We therefore investigated the biochemical interaction of AMPH-1 and RME-1 in membrane tubulation. Tubules generated from PtdSer-containing liposomes incubated with AMPH-1 and RME-1 in the presence of ATP-γ-S were qualitatively different from tubules generated by the individual proteins (Fig. 6e, e′). The most striking difference was in the reduction of tubule length produced by AMPH-1 and RME-1 (ATP-γ-S) together. Such tubules were about one-third the length of tubules produced by the individual proteins (Fig. 6f, g). In addition, in the presence of AMPH-1, the apparent RME-1 (ATP-γ-S) spiral coat on the tubules was more regular and closely spaced than in RME-1 (ATP-γ-S) tubules in the absence of AMPH-1 (Fig. 6h). The tubules produced by AMPH-1 and RME-1 (ATP-γ-S) together were more rigid and the decoration more pronounced in profile than those produced by the individual proteins (Fig. 6e′). Similar to our observation with 100% PtdSer-containing liposomes, upon incubation with 10% PtdIns(4,5)P_2-containing liposomes we found that a combination of AMPH-1- and RME-1 generated tubules that were dramatically shorter than those produced by the individual proteins (Fig. 7e, e′, g).

The physical interaction of AMPH-1 and RME-1 through the AMPH-1 Asn-Pro-Phe motifs seems critical for the formation of hybrid tubules. AMPH-1(F309A, F363A) was unable to form short tubules from PtdSer-containing liposomes when co-incubated with RME-1 (ATP-γ-S). Rather, long thin tubules equivalent to those formed from AMPH-1(F309A, F363A) alone dominated the reaction (Supplementary Information, Fig. S7). A few wide RME-1-type tubules were also observed but were relatively rare.

The ratio of AMPH-1 to RME-1 in the reaction mixture does not seem to control tubule length, as reducing AMPH-1 by 10-fold to 250 nM while keeping RME-1 levels constant (2.5 μM), produced many short PtdSer tubules that were similar in length to those produced by the proteins at a 1:1 stoichiometry. This suggests that AMPH-1 and RME-1 tend to assemble into a coat of a particular length, rather than one that varies in length depending on their relative available concentrations. (Supplementary Information, Fig. S7f, g).

RME-1 nucleotide state is critical for tubulation

Finally we investigated the effects of nucleotide state on the *in vitro* reaction. We found that RME-1 (ADP) lacked most tubulation activity in this assay, even though it still bound to PtdSer-containing liposomes (Fig. 8). Furthermore, we found that RME-1 (ADP) together with AMPH-1 added to PtdSer liposome preparations led to an approximately 7-fold decrease in tubulation capacity, including loss of most of the thin tubules characteristic of generation by AMPH-1 alone. This suggests that RME-1 in the inactive ADP-bound state interacts with AMPH-1 and prevents AMPH-1-mediated tubulation. Our RME-1 tubulation results are different from those reported for mammalian EHD2, the most diverged member of this protein family. EHD2 was found to be insensitive to nucleotide conditions in tubulating PtdSer-containing liposomes[9]. Although under more stringent binding conditions, with liposomes of lower PtdSer composition, EHD2 liposome tubulation was also dependent on nucleotide state[9].

DISCUSSION

The work of Daumke *et.al.*[9] and the work presented here, suggest that RME-1/EHD family proteins can function in membrane tubulation and potentially cause membrane fission through a self-assembly mechanism largely similar to that mediated by Dynamin. AMPH-1, through its BAR domain, could function to initiate endosome tubule formation and then recruit and activate RME-1 ATPase activity to drive tubule fission. Noteably, AMPH-1 seems to limit the assembly of RME-1 rings on membrane tubules. Recent work on the mechanism of Dynamin-mediated membrane fission indicates that short Dynamin spirals are the active agents of fission[40,41]. These studies found that long Dynamin assemblies constricted tubules but failed to promote fission upon GTP hydrolysis, whereas GTP hydrolysis and membrane release by short Dynamin assemblies frequently produced full fission. Thus, by limiting RME-1 spiral assembly, AMPH-1 may help to generate productive RME-1 assemblies. The AMPH-1 SH3 domain might interact with other endocytic regulatory proteins and help create a hub for protein interactions relevant for the RME-1 recycling function.

Another similarity of RME-1/EHD family proteins and Dynamin is that they interact with Syndapin (also known as Pacsin), a known activator of Wasp- and Arp2/3-mediated actin polymerization, suggesting that RME-1 family proteins may promote actin dynamics on endosomes to promote membrane fission[42]. Membrane-associated actin dynamics is thought to promote membrane fission by increasing membrane tension during Dynamin-mediated membrane constriction[43]. Further analysis of RME-1/EHD function is likely to provide important insights into membrane fission mechanisms that operate on endosomal membranes. □

METHODS

Methods and any associated references are available in the online version of the paper at http://www.nature.com/naturecellbiology/.

Note: Supplementary Information is available on the Nature Cell Biology website.

ACKNOWLEDGEMENTS

We thank P. McPherson, Z. Zhou, B. Kay, G. Prandergast and S. Mitani for important reagents. The monoclonal against RME-1 was made at Washington University School of Medicine and funded by Grant R24RR22234 (PI M. L. Nonet). We also thank C. Martin, P. Yurchenco, D. Winkelman, F. Matsumura, S. Yamashiro and S. H. deGregori for sharing their instruments, reagents and protocols; A. Shi for the construction and gift of the GFP–SDPN-1 strain; R. Patel and V. Starovoytov for expert assistance with electron microscopy protocols and Z. Pan for usage of the confocal microscopy facility; O. Daumke and T. Pucadyil for discussions and advice on liposome tubulation experiments; P. Schweinsberg for technical assistance. This work was supported by NIH Grants GM67237 to B.D.G and GM074876 to S.C., a NJCSCR Graduate Fellowship 06-2915-SCR-E-0, an Anne B. and James B. Leathem Fellowship, a McCallum Fund Fellowship Grant to S.P., an American Heart Association student fellowship to M.S. and a Rutgers Summer Undergraduate Research Fellowship (SURF) to K.P.

AUTHOR CONTRIBUTIONS

S.P. participated in experimental design, performed the *C. elegans*-related experiments and the biochemical and liposome experiments (Figs 1–4, 6–8 and Supplementary Information, Figs S1–5 and S7) and wrote the manuscript. M.S. performed the mammalian cell experiments (Fig. 5 and Supplementary Information, Fig. S6) and helped to write those sections of the manuscript. K.P. contributed to developing some strains used in the study. S.C. designed the mammalian cell experiments. C.M.C. designed the experiments related to liposome biochemistry and trained S.P. to do those experiments. B.D.G. designed the experiments, trained S.P. in all *C. elegans* experiments and wrote the paper.

COMPETING FINANCIAL INTERESTS

The authors declare no competing financial interests.

Published online at http://www.nature.com/naturecellbiology/.
Reprints and permissions information is available online at http://npg.nature.com/reprintsandpermissions/.

1. Grant, B. *et al.* Evidence that RME-1, a conserved *C. elegans* EH-domain protein, functions in endocytic recycling. *Nature Cell Biol.* **3,** 573–579 (2001).
2. Lin, S. X., Grant, B., Hirsh, D. & Maxfield, F. R. Rme-1 regulates the distribution and function of the endocytic recycling compartment in mammalian cells. *Nature Cell Biol.* **3,** 567–572 (2001).
3. Caplan, S. *et al.* A tubular EHD1-containing compartment involved in the recycling of major histocompatibility complex class I molecules to the plasma membrane. *EMBO J.* **21,** 2557–2567 (2002).
4. Lee, D. W. *et al.* ATP binding regulates oligomerization and endosome association of RME-1 family proteins. *J. Biol. Chem.* **280,** 17213–17220 (2005).
5. Naslavsky, N., Rahajeng, J., Sharma, M., Jovic, M. & Caplan, S. Interactions between EHD proteins and Rab11-FIP2: a role for EHD3 in early endosomal transport. *Mol. Biol. Cell* **17,** 163–177 (2006).
6. Sharma, M., Naslavsky, N. & Caplan, S. A role for EHD4 in the regulation of early endosomal transport. *Traffic* **9,** 995–1018 (2008).
7. Shao, Y. *et al.* Pincher, a pinocytic chaperone for nerve growth factor/TrkA signaling endosomes. *J. Cell Biol.* **157,** 679–691 (2002).
8. Guilherme, A. *et al.* EHD2 and the novel EH domain binding protein EHBP1 couple endocytosis to the actin cytoskeleton. *J. Biol.Chem.* **279,** 10593–10605 (2004).
9. Daumke, O. *et al.* Architectural and mechanistic insights into an EHD ATPase involved in membrane remodelling. *Nature* **449,** 923–927 (2007).
10. Sever, S. Dynamin and endocytosis. *Curr. Opin. Cell Biol.* **14,** 463–467 (2002).
11. Roux, A. & Antonny, B. The long and short of membrane fission. *Cell* **135,** 1163–1165 (2008).
12. Salcini, A. E. *et al.* Binding specificity and in vivo targets of the EH domain, a novel protein–protein interaction module. *Genes Dev.* **11,** 2239–2249 (1997).
13. Grant, B. D. & Caplan, S. Mechanisms of EHD/RME-1 protein function in endocytic transport. *Traffic* (2008).
14. Kieken, F., Jovic, M., Naslavsky, N., Caplan, S. & Sorgen, P. L. EH domain of EHD1. *J. Biomol. NMR* **39,** 323–329 (2007).
15. Takei, K., Slepnev, V. I., Haucke, V. & De Camilli, P. Functional partnership between amphiphysin and dynamin in clathrin-mediated endocytosis. *Nature Cell Biol.* **1,** 33–39 (1999).
16. David, C., McPherson, P. S., Mundigl, O. & de Camilli, P. A role of amphiphysin in synaptic vesicle endocytosis suggested by its binding to dynamin in nerve terminals. *Proc. Natl Acad. Sci. USA* **93,** 331–335 (1996).
17. Shi, A. *et al.* A novel requirement for *C. elegans* Alix/ALX-1 in RME-1-mediated membrane transport. *Curr. Biol.* **17,** 1913–1924 (2007).
18. Sato, K. *et al.* Differential requirements for clathrin in receptor-mediated endocytosis and maintenance of synaptic vesicle pools. *Proc. Natl Acad. Sci. USA* **106,** 1139–1144 (2009).
19. Chen, C. C. *et al.* RAB-10 is required for endocytic recycling in the *Caenorhabditis elegans* intestine. *Mol. Biol. Cell* **17,** 1286–1297 (2006).
20. Zhang, B. & Zelhof, A. C. Amphiphysins: raising the BAR for synaptic vesicle recycling and membrane dynamics. Bin-Amphiphysin-Rvsp. *Traffic* **3,** 452–460 (2002).
21. Razzaq, A. *et al.* Amphiphysin is necessary for organization of the excitation-contraction coupling machinery of muscles, but not for synaptic vesicle endocytosis in *Drosophila*. *Genes Dev.* **15,** 2967–2979 (2001).
22. Zelhof, A. C. *et al. Drosophila* Amphiphysin is implicated in protein localization and membrane morphogenesis but not in synaptic vesicle endocytosis. *Development* **128,** 5005–5015 (2001).
23. Leventis, P. A. *et al. Drosophila* Amphiphysin is a post-synaptic protein required for normal locomotion but not endocytosis. *Traffic* **2,** 839–850 (2001).
24. Grabs, D. *et al.* The SH3 domain of amphiphysin binds the proline-rich domain of dynamin at a single site that defines a new SH3 binding consensus sequence. *J. Biol Chem.* **272,** 13419–13425 (1997).
25. Burack, M. A., Silverman, M. A. & Banker, G. The role of selective transport in neuronal protein sorting. *Neuron* **26,** 465–472 (2000).
26. Naslavsky, N., Weigert, R. & Donaldson, J. G. Characterization of a nonclathrin endocytic pathway: membrane cargo and lipid requirements. *Mol. Biol. Cell* **5,** 3542–3552 (2004).
27. Naslavsky, N., Weigert, R. & Donaldson, J. G. Convergence of non-clathrin- and clathrin-derived endosomes involves Arf6 inactivation and changes in phosphoinositides. *Mol. Biol. Cell* **14,** 417–431 (2003).
28. Farsad, K. *et al.* A putative role for intramolecular regulatory mechanisms in the adaptor function of amphiphysin in endocytosis. *Neuropharmacology* **45,** 787–796 (2003).
29. McMahon, H. T., Wigge, P. & Smith, C. Clathrin interacts specifically with amphiphysin and is displaced by dynamin. *FEBS Lett.* **413,** 319–322 (1997).
30. Olesen, L. E. *et al.* Solitary and repetitive binding motifs for the AP2 complex alpha-appendage in amphiphysin and other accessory proteins. *J. Biol. Chem.* **283,** 5099–5109 (2008).
31. Owen, D. J. *et al.* Crystal structure of the amphiphysin-2 SH3 domain and its role in the prevention of dynamin ring formation. *EMBO J.* **17,** 5273–5285 (1998).
32. Slepnev, V. I. & De Camilli, P. Accessory factors in clathrin-dependent synaptic vesicle endocytosis. *Nature Rev. Neurosci.* **1,** 161–172 (2000).
33. Yoshida, Y. *et al.* The stimulatory action of amphiphysin on dynamin function is dependent on lipid bilayer curvature. *EMBO J.* **23,** 3483–3491 (2004).
34. Lee, E. *et al.* Amphiphysin 2 (Bin1) and T-tubule biogenesis in muscle. *Science* **297,** 1193–1196 (2002).
35. Muller, A. J. *et al.* Targeted disruption of the murine Bin1/Amphiphysin II gene does not disable endocytosis but results in embryonic cardiomyopathy with aberrant myofibril formation. *Mol. Cell. Biol.* **23,** 4295–4306 (2003).
36. Jovic, M., Kieken, F., Naslavsky, N., Sorgen, P. L. & Caplan, S. Eps15 homology domain 1-associated tubules contain phosphatidylinositol-4-phosphate and phosphatidylinositol-(4, 5)-bisphosphate and are required for efficient recycling. *Mol. Biol. Cell* **20,** 2731–2743 (2009).
37. Yamashiro, D. J., Tycko, B., Fluss, S. R. & Maxfield, F. R. Segregation of transferrin to a mildly acidic (pH 6.5) para-Golgi compartment in the recycling pathway. *Cell* **37,** 789–800 (1984).
38. Takei, K., Slepnev, V. I. & De Camilli, P. Interactions of dynamin and amphiphysin with liposomes. *Methods Enzymol.* **329,** 478–486 (2001).
39. Brown, F. D., Rozelle, A. L., Yin, H. L., Balla, T. & Donaldson, J. G. Phosphatidylinositol 4, 5-bisphosphate and Arf6-regulated membrane traffic. *J. Cell Biol.* **154,** 1007–1017 (2001).
40. Pucadyil, T. J. & Schmid, S. L. Real-time visualization of dynamin-catalyzed membrane fission and vesicle release. *Cell* **135,** 1263–1275 (2008).
41. Bashkirov, P. V. *et al.* GTPase cycle of Dynamin is coupled to membrane squeeze and release, leading to spontaneous fission. *Cell* (2008).
42. Braun, A. *et al.* EHD proteins associate with syndapin I and II and such interactions play a crucial role in endosomal recycling. *Mol. Biol. Cell* **16,** 3642–3658 (2005).
43. Roux, A., Uyhazi, K., Frost, A. & De Camilli, P. GTP-dependent twisting of dynamin implicates constriction and tension in membrane fission. *Nature* **441,** 528–531 (2006).